Journal of Power Sources 195 (2010) 3166–3175

Contents lists available at ScienceDirect

Journal of Power Sources

journal homepage: www.elsevier.com/locate/jpowsour

Experimental verification of a membrane humidifier model based on the effectiveness method

David Kadylak[a], Walter Mérida[a,b,*]

[a] Clean Energy Research Centre, University of British Columbia, Vancouver, BC, Canada V6T 1Z4
[b] Institute for Fuel Cell Innovation, 4250 Wesbrook Mall, Vancouver, BC, Canada V6T 1W5

ARTICLE INFO

Article history:
Received 18 October 2009
Received in revised form 1 December 2009
Accepted 2 December 2009
Available online 6 December 2009

Keywords:
Humidifier
Membrane
Fuel cell
Effectiveness
Moisture transfer
Model verification

ABSTRACT

Experiments conducted on a commercial fuel cell humidifier determined that the water recovery ratio is the best performance metric because it considers the water supplied to the humidifier. Data from a porous polymer membrane with a hydrophilic additive were analyzed under a heat and mass transfer model. The membrane showed low water uptake profiles at relative humidities below 80 percent, and a steep increase in water uptake above threshold.

The experiments were conducted with samples of the porous membrane in a single cell humidifier at isothermal conditions at temperatures of 25, 50, and 75 °C. The water recovery ratio for the porous membrane decreased with increasing flow rate.

The model was verified experimentally and its predictions agreed with the measured data.

1. Introduction

Reactant humidifiers are required in the balance of plant of a fuel cell system, and they represent as much as 20% of the total system cost [1]. Technological improvements to reactant humidifiers will help reduce the costs associated with fuel cell systems. Such improvements require fundamental understanding of the parameter effects on humidifier design to enable improved designs and lower costs. For optimal performance of a proton exchange membrane fuel cell (PEMFC), the membrane electrode assembly (MEA) requires hydration, and the membrane's conductivity depends on water content [2].

A humidifier is required to ensure that the cathode reactant gas, usually air, is hydrated before entering the fuel cell. Dry membrane operation or improper hydration causes performance degradation and premature failure due to changes in mechanical loading, and possible in pinholes [3,4]. A typical membrane such as Nafion swells by 10% upon hydration, and up to 20% or more at high temperatures; if there is improper humidification the continual swelling and contracting will induce mechanical stresses leading to membrane failure [5,6].

Fig. 1 illustrates the balance of plant for a PEM fuel cell system with a humidifier on the cathode side. Dry air is supplied from a compressor or blower to the dry inlet of the humidifier. As the dry incoming stream passes over the humidifier membrane it is humidified and heated from the wet inlet stream, which is coming from the fuel cell cathode exhaust. The humidified air then exits the humidifier as the humidified dry outlet stream and enters the fuel cell cathode to hydrate the MEA. Finally, the humidifier wet outlet stream exits the humidifier at a lower temperature and humidity than when it entered the humidifier, having supplied moisture and heat across the membrane.

Absolute metrics that are based on the total amount of water transferred can be defined on a mass or molar basis. The total water transfer rate $\dot{m}_{H_2O}$ is simply the rate of water mass transferred across the membrane (e.g., in kg s^{-1}, or kg m^{-2} s^{-1}). A perfect humidifier would have a water transfer rate equal to the flow rate of water being supplied to the wet inlet of the humidifier. This amount can be determined from the humidity and saturation temperature and the air flow rate.

The dew point approach temperature (DPAT) is a measure based on available humidity. It is defined by the difference between the

Abbreviations: AFM, atomic force microscopy; ERV, energy recovery ventilator; FTIR, Fourier transform infrared; HVAC, heating ventilating and air conditioning; MEA, membrane electrode assembly; PEM, proton exchange membrane; PEMFC, proton exchange membrane fuel cell; PFSA, perfluorosulfonic acid (i.e., Nafion™); PTFE, polytetrafluoroethylene (i.e., Teflon™).

* Corresponding author at: Clean Energy Research Centre, University of British Columbia, 6250 Applied Science Lane, Vancouver, BC, Canada V6T 1Z4.
Tel.: +1 604 822 4189; fax: +1 604 822 2403.
E-mail address: walter.merida@ubc.ca (W. Mérida).

0378-7753/$ – see front matter © 2009 Elsevier B.V. All rights reserved.
doi:10.1016/j.jpowsour.2009.12.005

Nomenclature

a	thermodynamic activity
C	constant parameter for sorption curve equation
d	channel depth (m)
D_h	hydraulic diameter (m)
D_{wm}	diffusivity of water in membrane ($kg\,m^{-1}\,s^{-1}$)
DPAT	dew point approach temperature
J	water flux ($kg\,s^{-1}\,m^{-2}$)
$\dot{m}$	mass flow rate ($kg\,s^{-1}$)
n	number of channels in humidifier plate
NTU	number of transfer units
P	pressure (Pa)
Q	volumetric flow rate (SLPM)
R^2	coefficient of determination for least-squares fit
Re	Reynolds number
R_L	ratio of mass flow capacity, minimum to maximum
T	temperature (K)
U_{eff}	effective mass transfer coefficient ($kg\,m^{-2}\,s^{-1}$)
w	width of channel (m)
WRR	water recovery ratio

Greek symbols

ε	effectiveness [0,1]
θ	water uptake ($kg\,H_2O\,kg^{-1}$ dry membrane)
θ_{max}	maximum water uptake capacity ($kg\,H_2O\,kg^{-1}$ dry membrane)
μ	dynamic viscosity ($kg\,m^{-1}\,s^{-1}$)
ρ	density ($kg\,m^{-3}$)
ω	absolute humidity (humidity ratio) ($kg\,H_2O\,kg^{-1}$ dry air)

Subscripts

air	air species
d	referring to the dry (or sweep) side; dew point, when used with T
di	dry side channel inlet
do	dry side channel outlet
H_2O	water
iso	isothermal conditions
L	latent or moisture
mem, m	membrane
min	minimum
ref	reference state
w	referring to the wet (or feed) side
wi	wet side channel inlet
wo	wet side channel outlet

dew point temperatures at dry outlet and the wet inlet in the humidifier:

$$\mathrm{DPAT} = T_{d,wi} - T_{d,do} \tag{1}$$

For ideal an humidifier $T_{d,wi} = T_{d,do}$, and this assumes perfect heat and mass (water) transfer.

Another measure based on the available humidity is the water recovery ratio (WRR). This value describes how much water is transferred to the dry outlet compared to the amount of water supplied, which determines the maximum amount of water available for transfer:

$$\mathrm{WRR} = \frac{\dot{m}_{H_2O,do} - \dot{m}_{H_2O,di}}{\dot{m}_{H_2O,wi}} = \frac{(\omega_{do} - \omega_{di})\dot{m}_{air,d}}{\omega_{wi}\dot{m}_{air,w}} \tag{2}$$

For an ideal humidifier, WRR = 1.

If the air flow rates in each of the dry and wet streams are equal, the water recovery ratio reduces to:

$$\mathrm{WRR}\ (\dot{m}_{air,d} = \dot{m}_{air,w}) = \frac{\omega_{do} - \omega_{di}}{\omega_{wi}} \tag{3}$$

Recent humidifier modeling has been performed by Majsztrik et al. [7], Cave and Merida [8], Chen et al. [9], and Huizing et al. [10]. In regard to this work Park and Oh state "[these models] are difficult to apply in practice because of their complex forms. Hence, a simplified model is necessary and helpful to evaluate humidification. . .for PEM fuel cell applications" [11]. Park and Oh provide a comparable simple one-dimensional thermodynamic model for a liquid-to-gas Nafion membrane humidifier. Their model does not consider the convective effects of the flow in addition to the thickness-dependent membrane permeability.

Other authors have focused on the shell-and-tube design of Nafion membrane humidifiers [9,12,13]. However, fuel cell system integrators are seeking to replace Nafion as a membrane for PEMFC humidification due to its prohibitively high price (e.g., $\$500\,m^{-2}$ [14]). The work of Monroe et al. is primarily concerned with characterization of membranes, specifically quantifying the interfacial characteristics of Nafion using a simple experimental chamber where the feed gas is circulated and exchanged [15]. Monroe presented a method for obtaining a vaporization-exchange rate coefficient from water vapor permeation experiments for use in his model.

The empirical method applied by Huizing compares the theoretical diffusion time for liquid water from a membrane surface to the residence time of the water vapor in the humidifier [16]. A more detailed thermodynamic model is required to take into account the fundamental physical mechanisms affecting water transport.

The present experimental work builds on the previous work of Cave [17], but is applicable to various membranes. It uses a simpler method based on the effectiveness approach to heat exchanger design as applied to energy recovery ventilators (ERVs) [18].

Experiments are presented that first characterize the membranes via sorption curves, and analyze the best method to use as a performance metric applied to membrane humidifiers. Additional experiments with a widely available porous polymer membrane, yielded correlations that illustrate the model's ability to fit the experimental data and predict water transfer in membrane humidifiers.

2. Experimental

2.1. Experimental setup

2.1.1. Test station

Preliminary testing on the performance metric evaluations, and the effects of pressure and temperature parameters, was completed with a plate-and-frame membrane humidifier. The experimental setup used a G6820 test station from Greenlight Power, following the procedure outlined in Fig. 2 without the isothermal water bath. For these initial tests, a contact spray humidifier replaced the gas bubbler and gravimetric measurements replaced the dynamic humidity recordings (to obtain typical time-averaged water transfers over 10 min).

A more precise test station was used to conduct the model validation on the membrane. The experimental setup is shown in Fig. 2. Dry, compressed air from the laboratory is supplied to the back of the test station. A tee in the tubing was introduced to supply what would later become the wet and dry streams. For the dry stream, the air passes through a mass flow controller to regulate the flow rate. The dry air is then heated to the desired temperature, before entering the dry inlet port of the humidifier, which has been submerged in an isothermal water bath kept at a constant-temperature, T_{iso}.

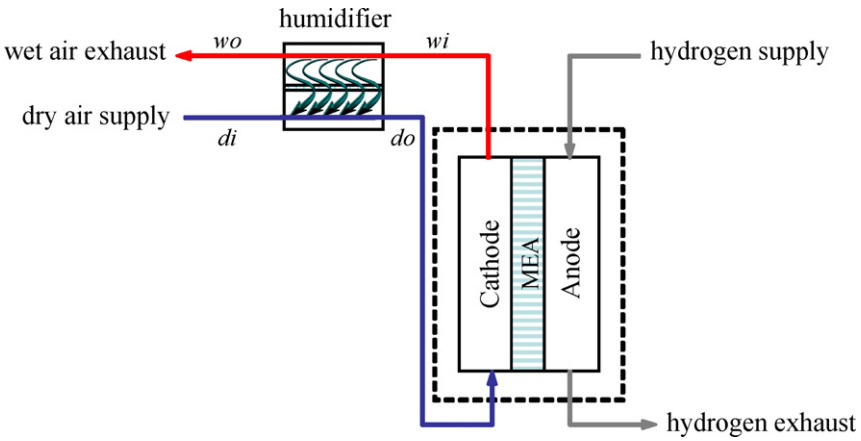

Fig. 1. Balance of plant of humidifier and fuel cell system.

For the wet stream, the compressed air first passes through a mass flow meter, then through a water gas bubbler, set at $T_{d,wi}$, where the stream's temperature will also be raised close to $T_d = T_{d,wi}$. It will then be conditioned to another temperature, T_{wi} which is generally higher than the dew point temperature $T_{d,wi}$ to prevent condensation. Both streams are vented to the atmosphere to prevent any backpressure, as indicated in Section 2.3. At the dry outlet a humidity sensor is placed in line with the stream to monitor and record the wet outlet temperature and humidity. The humidity sensor used is the HMT337 series of the Vaisala Humidicap humidity and temperature transmitter. The sensor has a dew point temperature accuracy of 1 °C or better in the range of test temperatures and at a relative humidity of at least 56% [19]. The casing enclosing this polymer-based capacitive humidity sensor is also placed in contact with the water in the water bath to maintain the same temperature, while preventing the sensor itself from becoming wet.

2.1.2. Humidifier

The humidifier used in the membrane and validation experiments was a single layer plate-and-frame cell as shown in Fig. 3. It was made from two plates of 2.5 cm thick acrylic, with $n = 7$ channels in parallel machined $d = 1$ mm deep. The channels are $w = 3$ mm wide and are separated by 1.5 mm lands. The flow enters and exits each side through push-connect elbow adaptors and then spreads out to seven channels. The membrane sample to be tested is placed in between each plate, with a 0.05 mm PTFE film creating a seal on either side of the membrane and acrylic plate. The entrance and exit areas of the membrane are covered with a thin sheet of water and air-impermeable polyimide film so that only the channel areas are exposed to the flow, eliminating any entrance and exit effects on water transfer and allowing the flow to become fully developed. The channel length exposed for water transport is $l = 135$ mm. Four ports have been made available to allow thermocouples to be placed into the flow and measure the temperature of each stream. A Type T thermocouple was placed through a hole drilled in a plastic pipe fitting plug.

A complete subscale prototype humidifier was used for the initial performance metric and parameter study tests. The humidifier was a dPoint Technologies $P \times 3$–46 mm consisting of 40 plates of 16 channels each, with a composite ionic membrane. The housing of the humidifier was made from polyester to provide rigid support and keep the humidifier insulated.

2.1.3. Isothermal conditioning

Isothermal conditions were necessary to prevent condensation within the test module, and the introduction of two-phase flow; another factor which is a challenge to model. Constant-temperature conditions allow for a controlled environment in which the water transfer can be isolated from any heat transfer that may occur in a humidifier, and focuses the study on the water transport across the membrane being tested. To this end, the humidifier was submerged in water contained in a heated water bath, along with the hollow adaptor which housed the humidity sensor. The connections were made as close as possible to the water level, hence the upright orientation as shown in Fig. 3. The water bath was kept at a temperature higher than the wet side dew point to prevent condensation when the test station feedback control overshot the dew point temperature set point. The inlet gas temperatures were also set higher than the dew point so as to prevent condensation, and the thermocouples placed in the humidifier at the inlet or outlet of each stream provided feedback for the test station gas temperature set point.

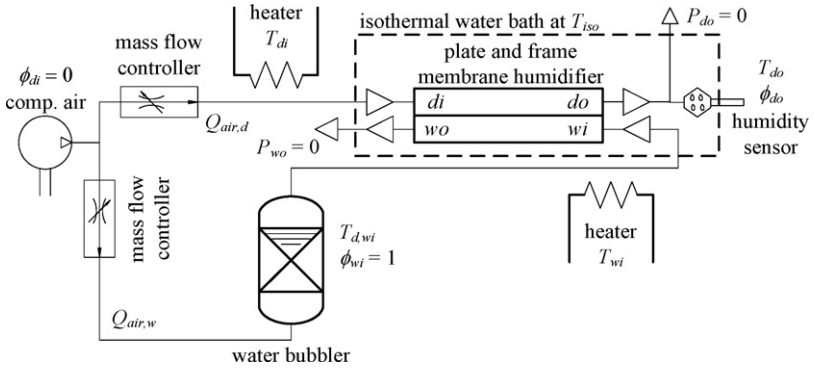

Fig. 2. Experimental setup of test station in line with test humidifier.

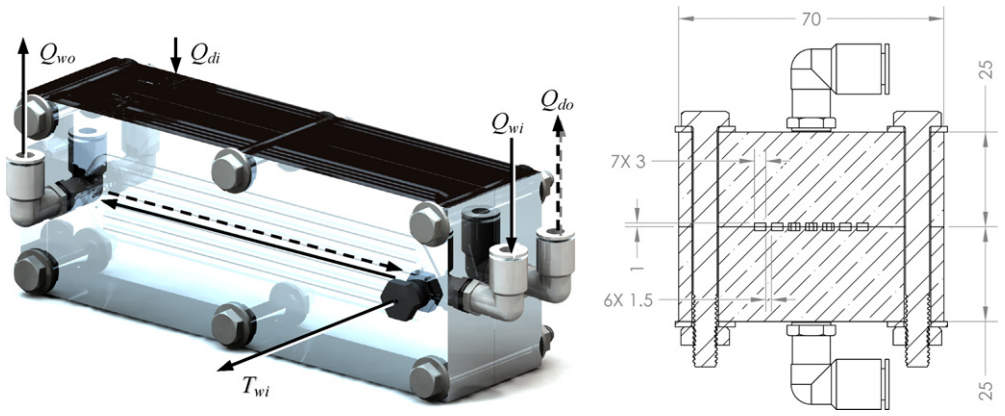

Fig. 3. Experimental single cell humidifier with installed ports and cross-section view.

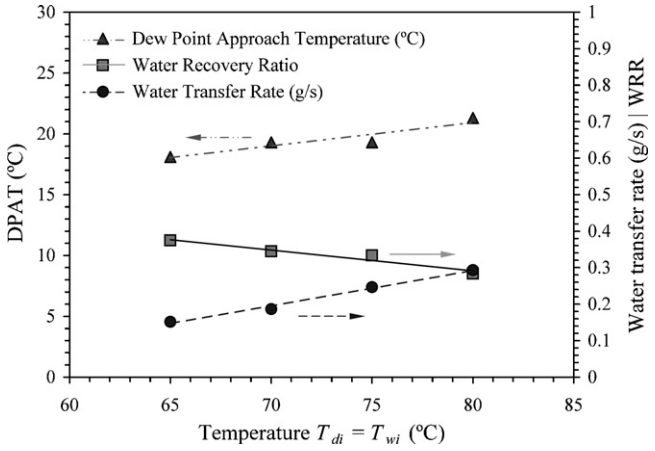

Fig. 4. Water transfer as operating temperature is changed.

2.2. Evaluation of performance measures

Experiments were conducted to determine how the humidifier performance varied with changes in operating temperature or in pressure differential across the membrane. To analyze the effects of these two operating conditions, the experiments were designed according to Table 1.

The first experiment was to run the humidifier with the wet and dry inlet streams set to equal temperatures, ranging from 65 to 80 °C, at 100 SLPM and no backpressure. The performance of the humidifier is plotted in terms of the water transfer rate ($\dot{m}_{H_2O}$), dew point approach temperature (DPAT), and water recovery ratio (WRR) in Fig. 4.

The DPAT compensates for using dew point temperature $T_{d,do}$ alone because the performance decreases in terms of DPAT as temperature increases, yet the actual dry outlet dew point temperature increases. Using the dry outlet dew point temperature only would be misleading, because an increase in dew point does not necessarily mean better performance. On the other hand, the water transfer rate is increasing as the temperature increases, but this can be explained by the additional water mass available to be transferred at higher saturated wet inlet temperatures. The water recovery ratio accounts for the extra water that is available as the temperature increases, and shows that the humidifier performance decreases in relative terms as the inlet temperatures increase.

In the second experiment, the dry inlet stream was kept at 25 °C and the wet inlet stream was supplied saturated at 65 °C, both streams with an air flow rate of 100 SLPM. This time the dry outlet backpressure was increased from ambient to 35 kPag, while keeping the wet outlet backpressure at atmospheric pressure, creating a pressure differential across the membrane of up to 35 kPa. This is equivalent to a pressure ratio of up to 1.35 (136 kPaa/101 kPaa). The dew point approach temperature, water transfer rate, and water recovery ratio are plotted in Fig. 5. In the previous experiment, the slopes of the DPAT and WRR linear fits had opposite signs, while in this experiment the slopes are both negative. In this case, the DPAT indicates that the humidifier is performing better as the pressure differential increases, yet both the water transfer rate and WRR suggest that the humidifier is actually performing worse as the pressure differential increases.

In conclusion, the dew point temperature or dew point approach temperature is a misleading measure of humidifier performance, and should be avoided. The problem is compounded by the nonlinear relation of water vapor pressure with temperature. In both experiments, the same membrane area was used, so the area-normalized water flux would give the same trend as the water transfer rate; their slopes will always be of the same sign. The absolute measure of water transfer rate does not adequately account for the change in available water at different flow conditions for the same humidifier; though it may be a good measure for comparing different humidifiers at the same operating conditions. A better

Table 1
Experimental matrix for performance measure evaluation.

Membrane	Control	Independent	Dependent
Ionic composite	$P_{do} = P_{wo} = 0$ kPag	$T_{di} = T_{wi} = 65 \ldots 80$ °C	WRR
	$\phi_{di} = 0\%$; $\phi_{wi} = 100\%$		WTR
	$Q_{air,d} = Q_{air,w} = 100$ SLPM		DPAT
Ionic composite	$T_{wi} = T_{d,wi} = 65$ °C	$P_{wo} = 0$ kPag $P_{do} = 0 \cdots 35$ kPag	WRR
	T_{di} = 25 °C; $T_{d,di}$ = −20 °C		WTR
	$Q_{air,d} = Q_{air,w} = 100$ SLPM		DPAT

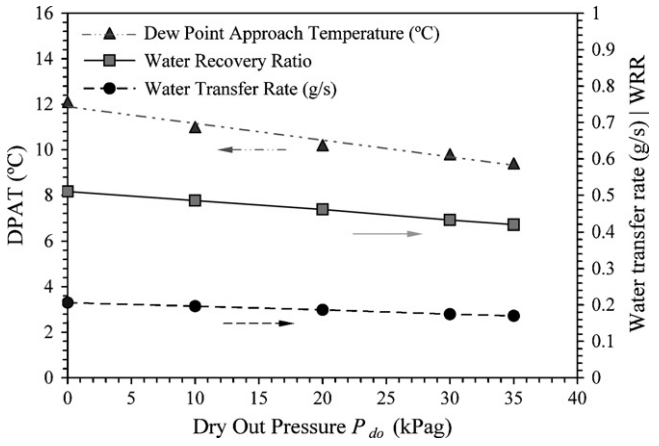

Fig. 5. Water transfer as dry stream pressure is changed.

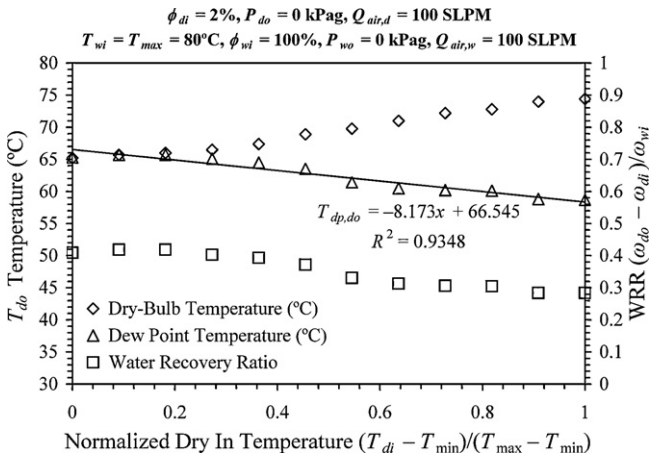

Fig. 6. Effect on water transfer of changing dry inlet temperature.

measure is the water recovery ratio, which takes into account the amount of water supplied as the operating conditions change; however, it is difficult to determine if an adequate amount of water is supplied to the fuel cell with the water recovery ratio alone. As with any other performance measure, a target minimum WRR would need to be calculated beforehand based on the operating conditions. Therefore, because the required operating conditions of the fuel cell will change with loading and the required amount of water or the minimum acceptable relative humidity will likewise change, it is proposed that water recovery ratio be used as the preferred performance metric. This measure is preferred because it will take into account the different amount of water supplied at each flow rate and flow conditions when the fuel cell power requirements change during operation.

2.3. Parameter effect study

A parameter sensitivity study was conducted with the plate-and-frame membrane prototype humidifier described in Section 2.1.2 above on the same Greenlight Power 5 kW G6820 test station.

The first test conducted in this study was to increase the dry incoming air temperature in increments of 5 °C until it met the wet in temperature, maintained at 80 °C, with ambient backpressures on both streams. The range of temperature was chosen such that it represented the typical range found in operating fuel cell temperatures, with the minimum temperature taken to be close to room temperature, or 25 °C. These dry inlet temperatures were normalized over the range of operating conditions to facilitate comparison with pressures in the subsequent experiments. The testing conditions are outlined in Table 2, and the results of the temperature-dependence test are displayed Fig. 6. Linear regression analysis of the dry outlet dew point against normalized temperature data demonstrates a slope of −8.17 °C (R^2 = 0.935).

The next test performed was to maintain constant inlet temperature while changing the dry air outlet backpressure from ambient to 35 kPa gauge. The range of pressure observed across the membrane is dictated by the pressure drop across a fuel cell stack, which is normally below 5 psi (35 kPa). These dry outlet pressures were

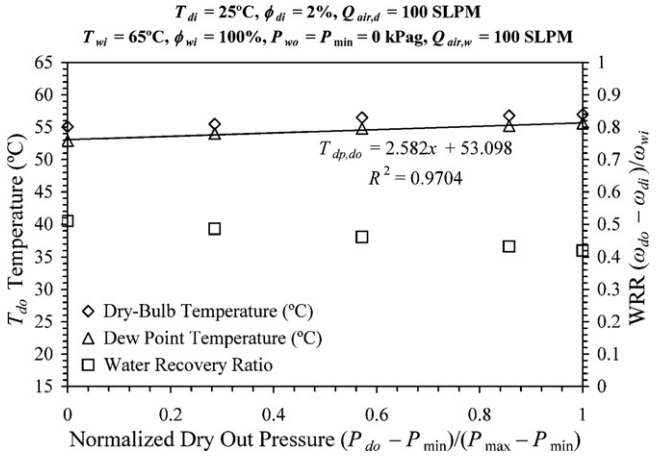

Fig. 7. Effect on water transfer of changing dry out backpressure, low total pressure.

normalized and the results of this test are shown in Fig. 7. Linear regression (R^2 = 0.97) through the dry outlet dew point temperature points in this graph gives a slope of 2.58 °C. Table 3 outlines the testing conditions of both pressure-dependence tests.

Operation at elevated pressures is required for many fuel cell systems, such as in automotive applications, so a similar test was performed at these pressures. Even at elevated pressures and automotive conditions, the PEM fuel cell stack will rarely develop pressure drops greater than 5 psi (35 kPa). In this test the dry outlet backpressure ranged from 120 to 155 kPag, while maintaining the wet outlet backpressure at 120 kPag. The outcome is displayed in Fig. 8. The dry side outlet pressures were likewise normalized in the plot.

At the high total pressures, the effect of changing the pressure in one gas stream has little effect on the water transfer. Likewise, at the lower total pressures – close to atmospheric pressure – comparing the slopes of the best fit lines reveals that the temperature difference between the inlets of the streams plays a larger role on water transfer than pressure difference between streams for the range

Table 2
Experimental matrix for temperature-dependence testing.

Membrane	Control	Flow Rate	Temperature (T_{di})	Dependent
Ionic composite	$T_{wi} = T_{d,wi} = 80$ °C	100 SLPM	25. . .80 °C	WRR
	$T_{d,di} = -20$ °C			T_{do}
	$P_{do} = P_{wo} = 0$ (gauge)			$T_{d,do}$

Table 3
Experimental matrix for pressure-dependence testing.

Membrane	Control	Pressure (kPag)			Dependent
		P_{wo}	$P_{do,\min}$	$P_{do,\max}$	
Ionic composite	$T_{wi} = T_{d,wi} = 65\ ^\circ C$	0	0	35	WRR
	$T_{di} = 25\ ^\circ C$; $T_{d,di} = -20\ ^\circ C$				T_{do}
	$Q_{air,d} = Q_{air,w} = 100$ SLPM				$T_{d,do}$
Ionic composite	$T_{wi} = T_{d,wi} = 65\ ^\circ C$	120	120	155	WRR
	$T_{di} = 25\ ^\circ C$; $T_{d,di} = -20\ ^\circ C$				T_{do}
	$Q_{air,d} = Q_{air,w} = 100$ SLPM				$T_{d,do}$

of temperature differences and pressure differences seen in practical fuel cell operation. Therefore, temperature effects were the focus of the present work. The effect of pressure will be neglected hereinafter. All the simulations and experiments were conducted at atmospheric pressure only.

2.4. Membrane characterization

Much testing and data have been collected on Dupont Nafion™ membranes in industry and in the literature. However, due to their high cost they are not expected to be used in future humidifier systems, hence the need to acquire more commercially feasible membranes as outlined in the Introduction. Furthermore, there are disparate data on Nafion's sorption and diffusivity values in the literature, as reported by Cave [17], making it difficult to use for practical modeling.

We report on a commercially available, porous membrane. The membrane is made from a polymer with a hydrophilic filler. It has a porosity of approximately 70%, thickness of 0.15 mm, and hydrophilic additive to polymer ratio of 2.5. It contains 15% plasticizer mineral oil used in the extrusion process. Due to its commercial availability, this membrane's cost is in the range of \$3 m^{-2}. The membrane is coated in a 4% Nafion (PFSA) DE2021 dispersion to decrease the air crossover, and baked at 100 °C for 1 h to help anneal the Nafion. Such a process adds about \$80 m^{-2} if coated on both sides, but a new functional polymer coating is being developed which currently only adds \$1 m^{-2}.

Three samples of the porous polymer with hydrophilic additive membrane were characterized using a vapor sorption instrument according to Ref. [20]. The sorption and desorption curves were characterized at 25 °C. Each sample was first dried to <1% relative humidity to determine its dry mass. The relative humidity was then increased stepwise in 10% increments up to 90%, then to 94% and 97%. The relative humidity was then decreased following the same profile to obtain the desorption curve. Mass equilibrium was obtained at each step before moving on to the next humidity setting. Mass equilibrium was reached when the change in mass with respect to total mass of the sample was less than 0.1%, or $dm/dt < 0.001$. The sorption and desorption profiles were discovered to be nearly equal. All six profiles (three absorption and three desorption) of the porous polymer-hydrophilic additive membrane with PFSA coating were averaged and are plotted with their 95% confidence interval error bars in Fig. 9.

A third-degree polynomial was used to curve fit the data up to 80% relative humidity, with an R^2 value of 0.996. The curve past 80% relative humidity is then fitted to a general isotherm curve for water uptake θ:

$$\theta = \frac{\theta_{\max}}{1 - C + C/\phi} \tag{4}$$

where the maximum moisture content is $\theta_{\max} = 2.5$, and the value of constant $C = 148$. With a value of C in the order of 100, indicating a low uptake for most of the low end of relative humidity and a sharp slope at the very high end of relative humidity, this porous membrane is characterized as Type III Extreme (Type IIIE) [21]. Several desiccant polymers exhibit Type III behavior, with a great increase in uptake only at values greater than 90% relative humidity [22].

2.5. Experimental design

In fuel cell humidification the wet stream entering the humidifier is generally saturated. Heat transfer occurs when there is a difference in temperature. Thus, water condensation, and two-

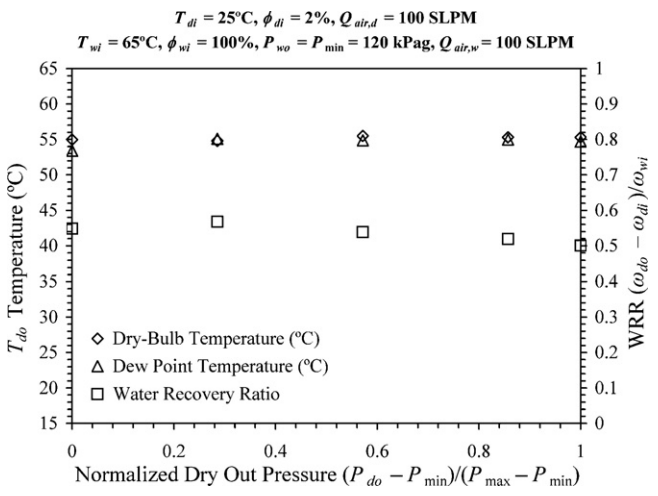

Fig. 8. Effect on water transfer of changing dry out backpressure, high total pressure.

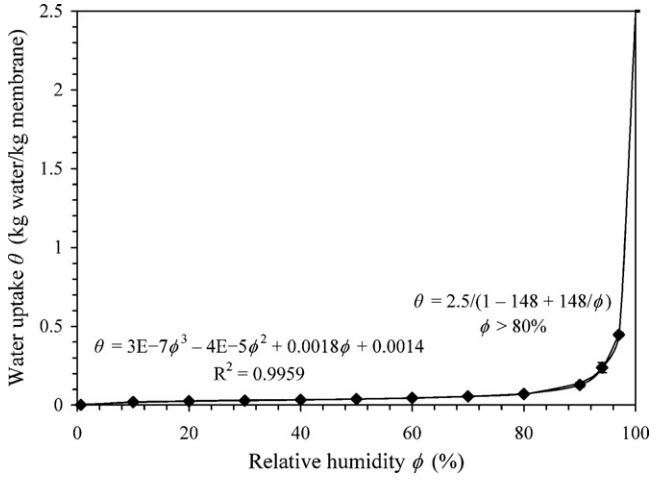

Fig. 9. Sorption isotherm at 25 °C of hydrophilic additive-impregnated porous polymer membrane, plasticizer intact, PFSA coated.

phase flow are inevitable with temperature difference between the flows or the surroundings. To maintain a comparison with past tests with modeling HVAC energy recovery ventilator (ERV) systems – upon which the current model is adapted – which do not have two-phase flow, isothermal conditions are chosen to perform comparison of performance. Another reason to keep isothermal conditions is to avoid higher levels of complexity when modeling that prevent convergence to a solution, and maintaining repeatable conditions during experiments.

Since the sorption curves were obtained at 25 °C, one set of experiments was conducted at a benchmark temperature of 25 °C, even though fuel cell systems typically operate at higher temperatures. Additional isothermal experiments were conducted at 50 and 75 °C. The choice of temperatures was based on the typical operating conditions in target applications (mobile, backup power, etc.).

It is necessary to test a range of flow rates; both because the humidifier will be exposed to different demands as the fuel cell operates through a range of power, and because it is required in determining the rated flow of a certain humidifier design. Due to the large number of plates to divide the flow, a plate-and-frame humidifier will always run at laminar flow, even though design elements may be introduced to cause flow separation and therefore enhance heat and mass transfer. A particular plate-and-frame humidifier designed for backup power applications may enable a Reynolds number of 80. The proposed test jig for the humidifier experiments has 7 channels with $d = 1$ mm height and $w = 3$ mm width, with one layer for each stream. The hydraulic diameter, D_h, is found from:

$$D_h = \frac{4wd}{2(w+d)} = 1.5\,\text{mm} \tag{5}$$

The Reynolds number is defined as

$$Re = \frac{\rho D_h Q}{\mu w d} \tag{6}$$

Eq. (6) can be rearranged to find the flow rate per channel, Q, using the 75 °C isothermal case to obtain the dynamic viscosity of air $\mu = 2.07 \times 10^{-5}\,\text{kg m}^{-1}\,\text{s}^{-1}$, and its density at STP $\rho = 1.29\,\text{kg m}^{-3}$:

$$Q = \frac{Re\mu wd}{\rho D_h} = 0.154\ \text{SLPM} \tag{7}$$

The flow rate per stream is found by multiplying by the number of channels, $n = 7$, so that the flow rate for each side is 1.08 SLPM. An Arbin 50 W Fuel Cell Test Station (FCTS), which has mass flow controllers rated up to 1.1 SLPM and 2 SLPM for two separate streams, was used to supply metered dry air and saturated wet air. With the limitation of 1.1 SLPM of one stream in mind, the flow rates to be tested are at 0.4, 0.7, and 1 SLPM.

The dry stream of the humidifier will be at a higher air flow than the air flow of the wet stream because the air component coming out of the fuel cell stack will have depleted oxygen content, having reacted with hydrogen to form water; however, the ratio of air flows on the dry side compared to the wet side varies according to the stoichiometry used to supply the fuel cell with extra oxygen reactant. The higher the air stoichiometry supplied, the closer the air flow rate on the dry side will be to the air flow on the wet side. For this reason, a simplification is applied where the dry side and wet side air flows are maintained equal. Water is added to the wet side air flow from a gas bubbler to saturate the air at the given test temperature, and this water flow rate is not included in the test conditions as wet air does not pass through the mass flow controller. The dry air is supplied from a compressed air line, which has been measured to have a relative humidity between 0.16% and 2.9% through the whole test temperature range (or always lower than a −20 °C dew point temperature).

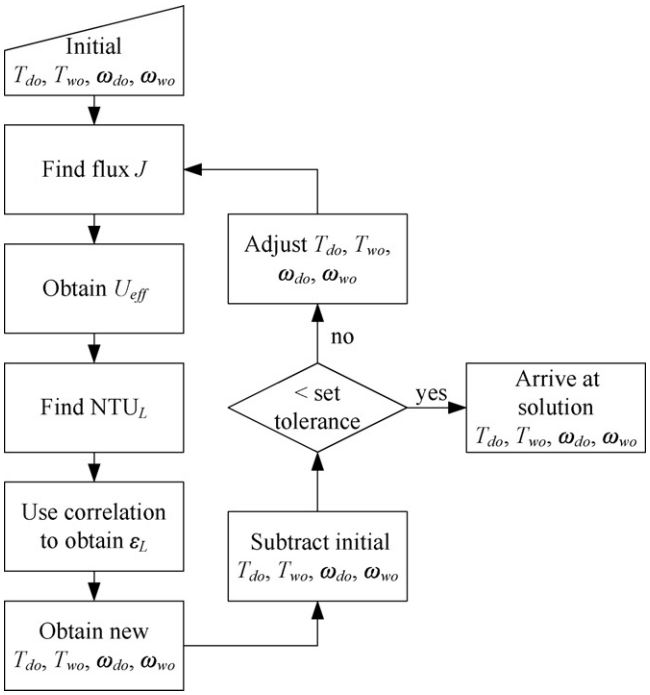

Fig. 10. Procedure for solving humidifier outlet conditions.

From the conclusions of Section 2.3, the focus of the study was on the temperature effects on water transport in practical operation, so the outlets are kept at ambient pressure. Since the chosen performance measure to be tested is the water transfer from the wet side to the dry side, the water recovery ratio (WRR) is the dependent variable in the tests. The amount of water at the dry outlet will also be presented by the dry outlet dew point $T_{d,do}$ as a measure of the amount of water available to the fuel cell, which is one of the parameters available from the humidity sensor. All the foregoing variables and testing conditions as inputs and the output are laid out in the test matrix of Table 4.

3. Model

We have previously reported on a heat and mass transfer model based on the effectiveness-number of transfer units method widely used in heat exchanger design [18]. The process of solving for the outlet absolute humidities is presented in the flow chart of Fig. 10, and it can be summarised as follows:

Table 4
Experimental testing matrix.

Membrane	Control	Flow rate	Temperature (T_{iso})			Dependent
Porous polymer PFSA coated	$T_{di} = T_{wi} = T_{d,wi} = T_{iso}$	0.4 SLPM	25 °C	50 °C	75 °C	WRR
	$T_{d,di} = -20$ °C	0.7 SLPM	25 °C	50 °C	75 °C	($T_{d,do}$)
	$P_{do} = P_{wo} = 0$ (gauge)	1 SLPM	25 °C	50 °C	75 °C	

- Solve seven non-linear equations (three flux, two humidity relations, and two water uptake) simultaneously to find the flux of water J.
- Find the effective mass transfer coefficient U_{eff}.
- Use U_{eff} in place of the common U_L in the equation used to find NTU_L.
- The latent effectiveness ε_L is now found from a common correlation, such as the correlation for unmixed cross-flows in a heat and humidity exchanger [18]:

$$\varepsilon_L = 1 - \exp\left[\frac{\exp(-\mathrm{NTU}_L^{0.78} R_L) - 1}{\mathrm{NTU}_L^{-0.22} R_L}\right] \quad (8)$$

- The outputs can now be found from the following equation:

$$\omega_{do} = \omega_{di} - \varepsilon_L \frac{(\dot{m}c_p)_{\min}}{(\dot{m}c_p)_d}(\omega_{di} - \omega_{wi}) \quad (9)$$

The model yielded a thermodynamic membrane humidifier model amenable to PEM fuel cell conditions based on the heat exchanger effectiveness method. Due to the elevated temperatures used in PEM fuel cells as compared to ERV systems and the non-linear dependence of the water saturation curve on temperature, the limitations were addressed in order to use the latent effectiveness method for PEMFC membrane humidifiers.

The new procedure was applied to three membrane types (Type I, linear, and Type III) and compared to the curves of latent effectiveness and latent NTU found using an ERV method. In fuel cell operation, the most likely conditions for the incoming wet and dry streams will be 100% and close to 0% relative humidity, respectively. For a 70 °C isothermal case, the technique yielded an enhancement in latent effectiveness of 29% for Type I membranes, 23% for linear-type membranes, and 46% for Type III membranes as compared to the ERV method [18].

4. Results and discussion

Three samples of the polymer with hydrophilic additive, Nafion-coated membrane were tested at three different flow rates and at three different temperatures according to the conditions presented in the experimental matrix, Table 4, for a minimum of 27 tests. The humidifier performance in terms of water transfer through the membrane is presented in Fig. 11 with the measured dry outlet dew point temperature, and the converted water recovery ratio.

As expected, the trend at all temperatures shows an inverse relation between flow rate and water transfer: as the flow rate increases, the water transfer relative to amount of supply water will decrease. In terms of water recovery ratio, the effect of decreasing water transfer with increasing flow rate is more pronounced the lower the temperature, which can be seen with the steeper slopes as temperature decreases. This effect may be more prominent at lower temperatures due to a lower saturation concentration of water at lower temperatures, as evidenced in the saturated vapor pressure curve. Likewise, humidifier performance suffers at higher temperatures, with water recovery ratios between 31% and 42% at the tested flow rates and geometry for the 75 °C isothermal condition, compared to the 46–69% WRR at 25 °C.

A proper, complete model requires membrane properties to be defined. A diffusion coefficient correlation is the only parameter that remains to be determined; so the diffusion coefficient is treated as a fitted parameter to the data. The temperature chosen to obtain the diffusion coefficient is 25 °C, where there is the most confidence in the data. For the polymer-hydrophilic additive membrane, the experimental data point with the least variance occurs at 0.7 SLPM with a standard error of 0.042 °C dew point. The diffusion coefficient for the porous polymer membrane was determined to be

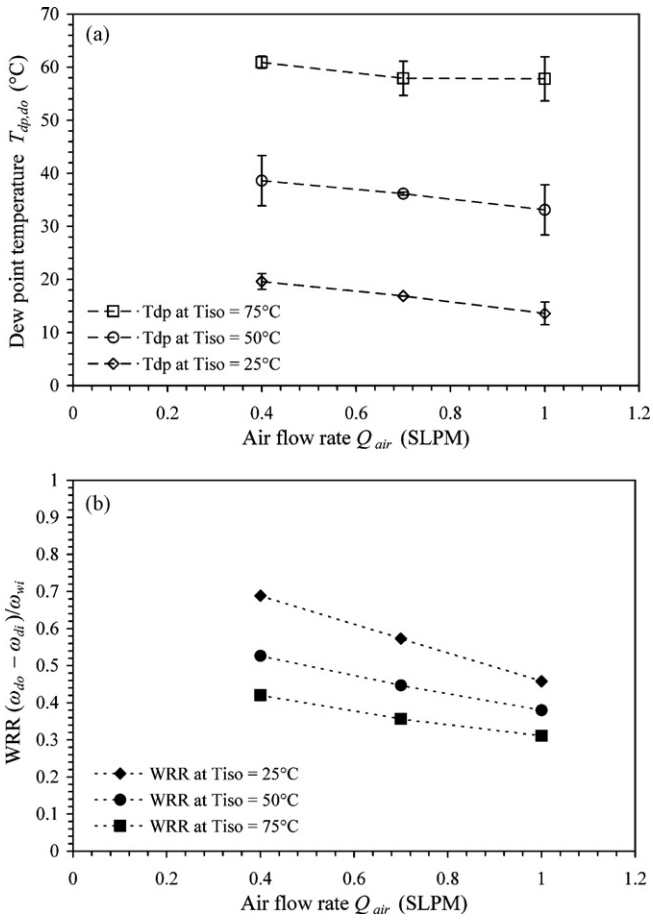

Fig. 11. Experimental results for porous polymer membrane.

$D_m = 9.42 \times 10^{-10}\ \mathrm{m^2\ s^{-1}}$. As a reference, Chen and Peng reported the diffusion coefficient for Nafion 115 (0.127 mm thick) to vary between $9.12 \times 10^{-11}\ \mathrm{m^2\ s^{-1}}$ and $3 \times 10^{-10}\ \mathrm{m^2\ s^{-1}}$ [13].

The diffusion coefficient also needs to be fitted at different temperatures. As a first approximation, the diffusion coefficient as a function of temperature can be modeled by an Arrhenius relation with activation energy E_a, as also found implemented in the literature for Nafion [23]:

$$D_{wm} = D_m \exp\left[\frac{E_a}{R}\left(\frac{1}{T_{ref}} - \frac{1}{T_m}\right)\right] \quad (10)$$

The reference temperature T_{ref} is 298.15 K, the temperature at which D_m was found for the first point. Once the temperature-dependence of the diffusion coefficient is applied to the data, as shown in Fig. 12, the activation energy for the polymer-hydrophilic additive membrane is found to be 24 300 J mol^{-1}. The activation energy for the tested membrane is of the activation energies in the literature for Nafion of 20 096 J mol^{-1} [23] and 18 003 J mol^{-1} [24]. Chen et al. also report higher activation energy than Yeo and Eisenberg from their tests with liquid-to-air membrane humidification [9]. The applicability of expressions like Eq. (10), and the validity of Arrhenius relationships are limited by gaps in our current understanding of the overall water transport processes in Nafion membranes.

Water sorption measurements have uncovered differences in water uptake from liquid and vapor environments. Several authors [25,26] have used the term "Schroeder's paradox" to describe the discrepancy. The paradox arises because the thermodynamic water activity is unity in both cases, but the equilibrium water uptake is

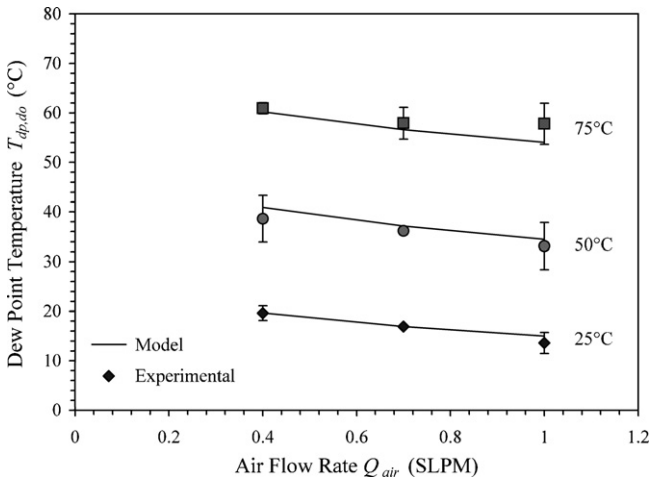

Fig. 12. Model comparison to experimental data for porous polymer with hydrophilic additive membrane, at ♦ T_{iso} = 25 °C, ● 50 °C, ■ 75 °C.

higher for membranes in contact with the liquid phase (e.g., 22 water molecules per sulfonic site instead of 14 as is the case for the vapor).

The majority of the investigations suggest that this difference is related to the physical structure of the membrane. For example, Zawodzinski et al. [27] reported that the membrane's surface becomes hydrophobic when the surrounding environment is water vapor. A phase inversion has also been observed by FTIR surface spectroscopy measurements reported earlier [28]. Gottesfeld et al. and Futerko and Hsing [29,30] agreed that the membrane remains in a stable thermodynamic state when it is equilibrated with vapor.

All the reports based on gravimetric measurements found differences between liquid and vapor water uptakes. Several physical explanations have contributed to the debate on whether the membrane changes its structural properties due to the chemical potential of the environment. Futerko and Hsing [30] proposed an explanation based on the Flory–Huggins model, which is based on the heat of mixing and entropy during the water uptake.

Similarly, McLean et al. [31] studied the ionic domains on or near the surface of K^+ type Nafion membranes at room temperature and humidity using atomic force microscopy (AFM). They discovered that the membrane showed a thin hydrophobic layer of ca. 0.5 nm on the surface. The formation of a hydrophobic layer has been proposed by Majsztrik et al. [7] as an explanation for the lower water uptake in vapor sorption and permeation experiments.

Hinatsu et al. [26] observed that the thermal history defines the polymer structure and hence the water uptake capacity. More recently, Onishi et al. [32] completed long term measurements on water sorption where the membrane–vapor system, and their results presented no evidence of Schroeder's paradox with 23 water molecules per sulfonic site for both vapor saturated and liquid water equilibrated membranes. The authors explained that previous experimental measurements that claim the existence of Schroeder's paradox either have neglected the effect of the polymer thermal history, or have assumed an erroneous equilibrium before the long term dynamic membrane–vapor interactions have been completed.

The ability of Nafion membranes to transport water and ions is the focus of intense research efforts, including work in our laboratories [15,33]. However, the alternative materials discussed here (e.g., coated composites) are more economical and can enable the commercialization of humidifiers in fuel cell applications.

5. Conclusions

The experiments under varying water transfer parameters indicated that the water recovery ratio (WRR) is the most appropriate performance metric for fuel cell humidifiers. This is especially valid across flow conditions, because the WRR accounts for the amount of water supplied even as the fuel cell operating conditions may change.

Initial experiments demonstrated temperature effects are greater than pressure effects over the practical operating ranges found in PEM fuel cells (25–80 °C, and 0–35 kPag and 120–155 kPag, respectively). Temperature had three times the effect compared to pressure on the dry outlet dew point temperature in the particular tests conducted on a subscale humidifier.

Membrane characterization experiments revealed that the porous membrane had low water uptake profiles at relative humidities less than 80%, with the profiles increasing sharply after 80%, with a maximum water uptake of 2.5. The porous membrane showed a decrease in water transfer as the flow rate was increased in the single cell humidifier experiments. Likewise, as the isothermal test temperature was increased, the water recovery ratio decreased.

The relevant diffusion coefficients were extracted from only a single point out of nine from the experimental data by using an Arrhenius relation for temperature-dependence. The porous polymer membrane had a diffusion coefficient of 9.42×10^{-10} m^2 s^{-1}. With the appropriate activation energy in the Arrhenius equation using only one other data point, the model matched the experimental results closely across all tested flow rates and interposing temperatures (within a 95% confidence interval). The practical use of the thermodynamic model was thereby validated for the range of conditions tested.

Acknowledgements

The authors would like to acknowledge the Natural Sciences and Engineering Research Council of Canada for financial assistance. Many thanks to Tatyana Soboleva (at Simon Fraser University), for data from dynamic vapor sorption experiments We thank Chris Goodchild at dPoint Technologies for performing the required testing and collecting the data outlined in the parameter study and performance metrics study. We acknowledge James Dean, president of dPoint Technologies, for providing prototype humidifiers and collaborating in the research project.

References

[1] J. Sinha, S. Lasher, Y. Yang, Direct hydrogen PEMFC manufacturing cost estimation for automotive applications, in: TIAX LLC DOE Hydrogen Program Review, Arlington, VA, 2009, pp. 50–64.
[2] J. Larminie, A. Dicks, Fuel Cell Systems Explained, second ed., John Wiley & Sons, West Sussex, England, 2003.
[3] X. Huang, R. Solasi, Y. Zou, M. Feshler, K. Reifsnider, D. Condit, et al., J. Polym. Sci. B 44 (16) (2006) 2346–2357.
[4] H. Tang, S. Peikang, S.P. Jiang, F. Wang, M. Pan, J. Power Sources 170 (1) (2007) 85–92.
[5] M.B. Satterfield, J.B. Benziger, J. Phys. Chem. B 112 (12) (2008) 3693–3704.
[6] M.B. Satterfield, P.W. Majsztrik, H. Ota, J.B. Benziger, A.B. Bocarsly, J. Polym. Sci. B 44 (16) (2006) 2327–2345.
[7] P.W. Majsztrik, M.B. Satterfield, A.B. Bocarsly, J.B. Benziger, J. Membr. Sci. 301 (1) (2007) 93–106.
[8] P. Cave, W. Merida, J. Power Sources 175 (1) (2008) 408–418.
[9] D. Chen, W. Li, H. Peng, J. Power Sources 180 (1) (2008) 461–467.
[10] R. Huizing, M. Fowler, W. Mérida, J. Dean, J. Power Sources 180 (1) (2008) 265–275.
[11] S. Park, I.-H. Oh, J. Power Sources 188 (2) (2009) 498–501.
[12] S.-K. Park, S.-Y. Choe, S.-H. Choi, Int. J. Hydrogen Energy 33 (9) (2008) 2273–2282.
[13] D. Chen, H. Peng, J. Dyn. Syst. Meas. Control 127 (3) (2005) 424–432.
[14] G. Hoogers, Fuel Cell Technology Handbook, CRC Press, Boca Raton, FL, 2003, p. 4.13.

[15] C.W. Monroe, T. Romero, W. Mérida, M. Eikerling, J. Membr. Sci. 324 (1–2) (2008) 1–6.
[16] R. Huizing, Design and membrane selection for gas-to-gas humidifiers for fuel cell applications. M.A.Sc. thesis (2007).
[17] P. Cave, Membrane moisture transfer in fuel cell humidifiers. M.A.Sc. thesis (2007).
[18] D. Kadylak, P. Cave, W. Merida, Int. J. Heat Mass Transfer 52 (5–6) (2009) 1504–1509.
[19] Vaisala, Vaisala HUMIDICAP® Humidity and Temperature Transmitter Series HMT330 User's Guide, Vaisala Oyj, Helsinki, 2005, ch. 7.
[20] D.J. Burnett, A.R. Garcia, F. Thielmann, J. Power Sources 160 (1) (2006) 426–430.
[21] C.J. Simonson, R.W. Besant, Int. J. Heat Mass Transfer 42 (12) (1999) 2171–2185.
[22] J.L. Niu, L. Zhang, J. Membr. Sci. 189 (2) (2001) 179–191.
[23] S.C. Yeo, A. Eisenberg, J. Appl. Polym. Sci. 21 (4) (1977) 875–898.
[24] M.W. Verbrugge, E.W. Schneider, R.S. Conell, R.F. Hill, J. Electrochem. Soc. 139 (12) (1992) 3421–3428.
[25] T.A. Zawodzinski, C. Derouin, S. Radzinski, R.J. Sherman, V.T. Smith, T.E. Springer, J. Electrochem. Soc. 140 (4) (1993) 1041–1047.
[26] J. Hinatsu, M. Mizuhata, H. Takenaka, J. Electrochem. Soc. 141 (6) (1994) 1493–1498.
[27] T.A. Zawodzinski, S. Gottesfeld Jr., S. Shoichet, T.J. McCarthy, J. Appl. Electrochem. 23 (1) (1993) 86–88.
[28] P.C. Rieke, N.E. Vanderborgh, J. Membr. Sci. 32 (2–3) (1987) 313–328.
[29] S. Gottesfeld, T.A. Zawodzinski, in: R.C. Alkire, H. Gerischer, D.M. Kolb, C.W. Tobias (Eds.), Advances in Electrochemical Science and Engineering, Wiley-VCH, Weinheim, 1997, pp. 249–261.
[30] P. Futerko, I. Hsing, J. Electrochem. Soc. 146 (6) (1999) 2049–2053.
[31] R.S. McLean, M. Doyle, B.B. Sauer, Macromolecules 33 (17) (2000) 6541–6550.
[32] L.M. Onishi, J.M. Prausnitz, J. Newman, J. Phys. Chem. B 111 (34) (2007) 10166–10173.
[33] T. Romero, W. Mérida, J. Membr. Sci. 338 (1–2) (2009) 135–144.